

Thermolabile Noble Metal Precursors: $(\text{NO})[\text{Au}(\text{NO}_3)_4]$, $(\text{NO})_2[\text{Pd}(\text{NO}_3)_4]$, and $(\text{NO})_2[\text{Pt}(\text{NO}_3)_6]$ **

Mathias S. Wickleder,* Frauke Gerlach, Steffen Gagelmann, Jörn Bruns, Mandus Fenske, and Katharina Al-Shamery*

Noble metals play a crucial role in various fields of application, for example, as optical and electrical devices and as heterogeneous catalysts. For most of these applications, the metals have to be provided in a well-defined form to address the desired properties. For example, catalytic activity is usually strongly surface-dependent and the production of nanoparticles of the metals is often mandatory.^[1–5] A second example is the use of metals in electronic devices as conductor pathways, which requires well-defined depositions of the metals.^[6,7] Owing to this significant impact, several physical and chemical processes have been developed to allow for the deposition of noble metals in different shapes. Among these, chemical vapor deposition (CVD) is the most common chemical procedure, and numerous precursors are known, especially for the element gold.^[8–12] The drawback of CVD techniques is that organometallic compounds are usually used, leading to significant carbon contamination of the deposited metals.^[13–15] Recently we have shown that the nitylium nitrate $(\text{NO}_2)[\text{Au}(\text{NO}_3)_4]$ is a suitable thermolabile precursor for gold; this species was obtained from the reaction of elemental gold with N_2O_5 .^[16] The use of nitrogen oxides for the preparation of anhydrous nitrates can be traced back to the 1970s when Addison et al. reported first investigations, mainly based on N_2O_4 .^[17] The advantage of $(\text{NO}_2)[\text{Au}(\text{NO}_3)_4]$ as a precursor is that it does not contain carbon or chlorine, and that its decomposition leads only to volatile products besides the metal. Moreover, the nitrate can be dissolved in N_2O_5 , so that deposition of the precursor for example on surfaces is easy to perform. Interestingly, this precursor can not only be decomposed thermally but also using an electron beam, which allows the simple “writing” of gold structures.^[17,18] These results led us to investigate whether noble metals can generally be transformed into thermolabile nitrates using N_2O_5 . In the course of these investigations, we were able to prepare the palladium and

platinum compounds $(\text{NO})_2[\text{Pd}(\text{NO}_3)_4]$ and $(\text{NO})_2[\text{Pt}(\text{NO}_3)_6]$, and furthermore a new gold nitrate, $(\text{NO})[\text{Au}(\text{NO}_3)_4]$.

Red single crystals of $(\text{NO})_2[\text{Pd}(\text{NO}_3)_4]$ and yellow single crystals of $(\text{NO})[\text{Au}(\text{NO}_3)_4]$, both exhibiting a plate-shaped habit, form when the respective metals react with N_2O_5 at room temperature under inert conditions (Figure 1 a,b). It is



Figure 1. Microscope images of single crystals of the complex nitrates $(\text{NO})_2[\text{Pd}(\text{NO}_3)_4]$ (left), $(\text{NO})[\text{Au}(\text{NO}_3)_4]$ (middle), and $(\text{NO})_2[\text{Pt}(\text{NO}_3)_6]$ (right).

imperative that the N_2O_5 is very pure, because no reaction occurs if the N_2O_4 content in the anhydride is too high. The difference to the preparation of the nitylium compound $(\text{NO}_2)[\text{Au}(\text{NO}_3)_4]$ ^[16] that we have described earlier is that much less N_2O_5 is used here. Unexpectedly, elemental platinum does not react with N_2O_5 under these conditions, even if the metal is provided as fine powder. Therefore we attempted to apply various platinum compounds as starting material, and we finally succeeded by using $\text{H}_2[\text{Pt}(\text{OH})_6]$, which was prepared according to a literature procedure.^[19] This reaction afforded, again at room temperature, light yellow plates of $(\text{NO})_2[\text{Pt}(\text{NO}_3)_6]$ (Figure 1 c). The nitylium nitrates are extremely hygroscopic and have to be handled under the strict exclusion of moisture. Furthermore, the decomposition of $(\text{NO})_2[\text{Pt}(\text{NO}_3)_6]$ begins as soon as the compound is removed from the reaction mixture.

In the crystal structure of $(\text{NO})_2[\text{Pd}(\text{NO}_3)_4]$, the Pd atom is coordinated in a square-planar manner by four monodentate nitrate groups (Figure 2, left). The Pd–O distances are uniformly at about 201 pm and the O–Pd–O angles deviate not more than 2° from the ideally expected 90°. The N–O distances within the nitrate groups are significantly enlarged for those oxygen atoms that are bonded to the Pd atom. According to the site symmetry of the palladium atom, the complex $[\text{Pd}(\text{NO}_3)_4]^{2-}$ anions show inversion symmetry (C_i) and are located on the mid points of the unit cell edges (Figure 2, right). Charge balance is achieved by the NO^+ cations, which have a typical N–O distance of 109.4 pm.^[20]

The structure of the anionic complex $[\text{Au}(\text{NO}_3)_4]^-$ in $(\text{NO})[\text{Au}(\text{NO}_3)_4]$ is nearly identical to its palladium analogue.

[*] Prof. Dr. M. S. Wickleder, Dr. F. Gerlach, S. Gagelmann, J. Bruns, Dr. M. Fenske, Prof. Dr. K. Al-Shamery
 Carl von Ossietzky University of Oldenburg, Institute for Pure and Applied Chemistry
 Carl-von-Ossietzky Strasse 9–11, 26129 Oldenburg (Germany)
 E-mail: mathias.wickleder@uni-oldenburg.de
 Katharina.Al-Shamery@uni-oldenburg.de

[**] Financial support of the Deutsche Forschungsgemeinschaft, the Fonds der Chemischen Industrie, and the Stiftung Nordwestmetall is gratefully acknowledged. We thank Wolfgang Saak for the collection of the X-ray data.



Supporting information for this article is available on the WWW under <http://dx.doi.org/10.1002/anie.201106107>.

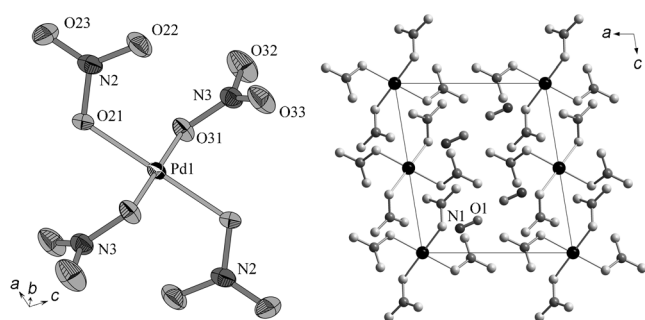


Figure 2. The $[\text{Pd}(\text{NO}_3)_4]^{2-}$ complex (left) and the crystal structure of $(\text{NO})_2[\text{Pd}(\text{NO}_3)_4]$ (right). Ellipsoids are set at 75% probability. Selected bond lengths [pm] and angles [$^\circ$]: Pd1–O21/O31 201.0(1)/201.1(1), N2–O21/O22/O23 131.4(2)/123.1(2)/122.8(2), N3–O31/O32/O33 131.7(2)/124.0(2)/121.5(2), N1–O1 104.9(2); O21–Pd1–O31 87.97(6)/92.03(6).

It shows also C_i symmetry and the square-planar coordination of the gold atoms is even closer to the ideal case with regard to the Au–O distances (200 pm) and the O–Au–O angles, which are essentially 90° (Figure 3, left). The strong asymmetry of

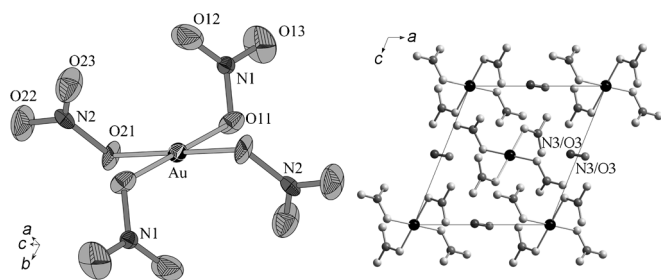


Figure 3. The $[\text{Au}(\text{NO}_3)_4]^-$ complex (left) and the crystal structure of $(\text{NO})[\text{Au}(\text{NO}_3)_4]$ (right). Ellipsoids are set at 75% probability. Selected bond lengths [pm] and angles [$^\circ$]: Au–O11/O21 200.3(7)/200.1(7), N1–O11/O12/O13 136(1)/124(1)/122(1), N2–O21/O22/O23 134(1)/121(1)/123(1), N3–O3 113(3); O11–Au–O21 90.0(3)/89.9(3).

the nitrate ions with respect to the N–O distances is also observed. The main difference in the crystal structures of the palladium and the gold nitrate is the arrangement of the complex anions with respect to each other, which is caused by the different charge and the reduced number of charge-balancing NO^+ cations in $(\text{NO})[\text{Au}(\text{NO}_3)_4]$. In contrast to the palladium compound, the NO^+ cations are located on special sites in the sense that a center of inversion is situated at the mid points of the N–O bonds ($2b$ site of space group $P2_1/n$). This position makes the nitrogen and the oxygen atom of the NO^+ dumbbells undistinguishable (Figure 3, right). It should be noted that $(\text{NO})[\text{Au}(\text{NO}_3)_4]$ is strongly related to its nityrium congener $(\text{NO}_2)[\text{Au}(\text{NO}_3)_4]$ where the NO_2^+ cation is located at the same position (with the nitrogen atom at the $2b$ site) as the NO^+ cation here.

The platinum(IV) nitrate $(\text{NO})_2[\text{Pt}(\text{NO}_3)_6]$ is the first example of a tetravalent platinum compound containing a complex oxoanion. Six nitrate groups are coordinated as monodentate ligands with the Pt–O distances falling in the narrow range of 199.9 to 200.9 pm (Figure 4, left). The

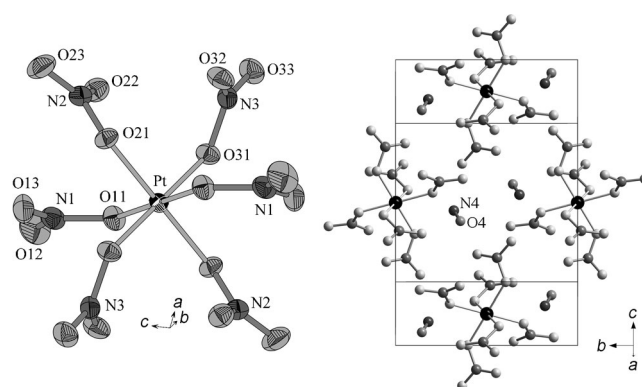


Figure 4. The $[\text{Pt}(\text{NO}_3)_6]^{2-}$ complex (left) and the crystal structure of $(\text{NO})_2[\text{Pt}(\text{NO}_3)_6]$ (right). Ellipsoids are set at 75% probability. Selected bond lengths [pm] and angles [$^\circ$]: Pt1–O11/O21/O31 199.9(2)/200.9(2)/200.3(2), N1–O11/O12/O13 134.2(3)/121.0(3)/121.6(4), N2–O21/O22/O23 135.0(3)/120.2(3)/122.3(4), N3–O31/O32/O33 133.8(3)/121.1(3)/121.8(3), N4–O4: 102.9(4); O11–Pt1–O21 101.14(7)/78.86(7), O11–Pt1–O31 100.93(7)/79.07(7), O21–Pt1–O31 101.56(7)/78.44(7).

resulting $\{\text{PtO}_6\}$ octahedron is remarkably distorted with respect to the O–Pt–O angles, which deviate in part more than 10° from the ideal value of 90° . Also in this compound there is a significant bond length variation within the nitrate groups, with the larger values found for the platinum-coordinated oxygen atoms. The complex $[\text{Pt}(\text{NO}_3)_6]^{2-}$ ions show inversion symmetry according to the $2d$ site of the Pt atom, and the NO^+ ions are located on a general crystallographic site, thus allowing a clear differentiation to be made between the N and the O atom (N–O: 102.9 pm).

The thermal decomposition of the complex noble metal nitrates as monitored by differential thermal analysis (DTA)/thermogravimetric analysis (TG) measurements show that the metals form in any case. $(\text{NO})_2[\text{Pd}(\text{NO}_3)_4]$ decomposes in a three-step process, with the first step already complete at 168°C . It can be attributed to the formation of $\text{Pd}(\text{NO}_3)_2$ according to the observed mass loss of 41.9% (calcd. 42.4%). The second step starts immediately after the first and leads to PdO at 298°C . The latter decomposes between 602 and 734°C and gives elemental palladium, as shown by its XRD pattern. For $(\text{NO})_2[\text{Pt}(\text{NO}_3)_6]$, the thermal analysis was carried out on samples containing N_2O_5 to avoid decomposition of the compound prior to the measurement. Thus, the first step of the observed decomposition is correlated to the release of adhesive N_2O_5 . Nevertheless, it seems to be certain that at least one intermediate is formed that is further degraded, leading to a platinum oxide (most reliably PtO_2), which finally leads to elemental platinum at a temperature of 550°C , according to X-ray analysis.

The decomposition of $(\text{NO})[\text{Au}(\text{NO}_3)_4]$ is already complete at about 240°C . The DTA/TG measurements show one quite strong but relatively broad signal ranging from 140 to 190°C and two significantly weaker effects with maxima at 200 and 215°C (Figure 5). The broad signal shows a shoulder indicating that the observed peak is in fact a superposition of two effects. Indeed, a DSC measurement of the compound made these two peaks visible, and the maxima could be found

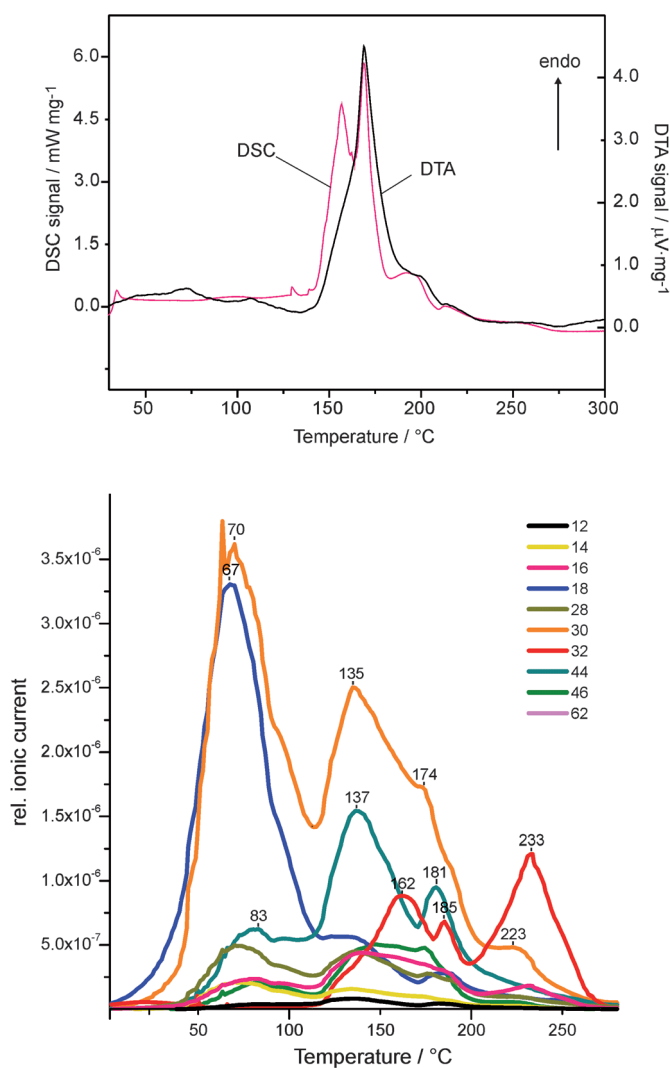


Figure 5. Thermal behavior of $(\text{NO})[\text{Au}(\text{NO}_3)_4]$: DSC and DTA data (upper part) show two closely associated strong signals, and two weak signals slightly below and above 200°C . According to thermal desorption measurements (TDS; lower part) the first step is dominated by the release of nitrogen oxides, while for the second step additionally O_2 is observed. Oxygen is also the dominant species for the last step. TDS curves show signals below 100°C as the sample was prepared in liquid N_2O_5 . A strong H_2O signal ($m/z = 18$) is attributed to contamination during sample preparation.

at 156 and 169°C . The weak peaks are also seen in the DSC curve, with maxima at 193 and 213°C . To investigate the decomposition behavior in more detail and to elucidate the precursor potential of $(\text{NO})[\text{Au}(\text{NO}_3)_4]$, we performed thermal desorption measurements (TDS) of samples that were deposited onto a silicon wafer as a solution in N_2O_5 . The ion signals upon heating can be divided in three regions. The first is clearly attributed to the release of solvent N_2O_5 and shows mainly ions with m/z at 30 (NO), 28 (N_2), and 44 (N_2O). Furthermore a signal at $m/z = 18$ indicates that some H_2O is formed, which is most likely due to the formation of HNO_3 during the sample preparation. The second region is associated with the precursor decomposition and shows the release of NO and N_2O and, after a small delay, also the occurrence of

O_2 . This region matches quite well the strong peaks observed in the DSC and DTA measurements. The third region in the TDS measurements is dominated by the signal for O_2 ($m/z = 32$) and is related to the weak peaks observed in the DSC curve. With respect to these findings, we assume that the decomposition of $(\text{NO})[\text{Au}(\text{NO}_3)_4]$ occurs via an oxide intermediate that readily decomposes further to yield elemental gold.

This assumption is also corroborated by XPS measurements (XPS = X-ray photoelectron spectroscopy) that were performed during the precursor decomposition (Figure 6). The spectrum at 350°C after complete decomposition of the

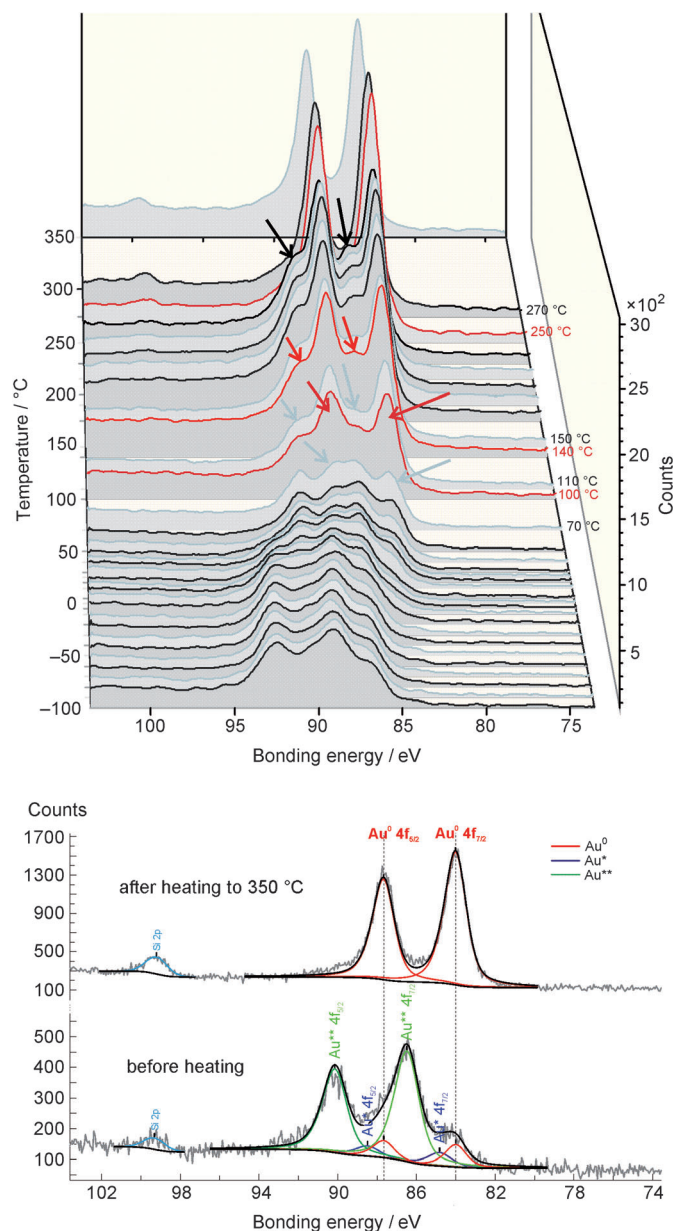


Figure 6. Temperature-dependent XPS on $(\text{NO})[\text{Au}(\text{NO}_3)_4]$, indicating the changes in energy for the $4f_{7/2}$ and $4f_{5/2}$ states of gold. The regions of strong changes are marked as red spectra and by arrows in the left diagram. Lower part: the spectra before and after heating of the precursor; the observed $2p$ signal for silicon did not change during the measurement and served as a standard during data handling.

precursor clearly shows the expected bonding energies of 84.0 and 87.7 eV for the Au4f_{7/2} and 4f_{5/2} states of elemental gold.^[23] The temperature region between 110 and 140 °C is dominated by the Au4f_{7/2} and 4f_{5/2} signals at 85.7 and 86.4 eV, respectively, which can be assigned to a gold oxide from the findings of the TDS measurements. When compared to literature data, this gold oxide is most probably Au₂O₃,^[23] but there are also some reports claiming bonding energies for oxidic Au^I species in the same region.^[24] However, reliable data are not available because Au₂O is still elusive. The spectra at temperatures before the precursor decomposition starts show energies at 86.5 and 90.2 eV, which can be attributed to 4f_{7/2} and 4f_{5/2} states of Au³⁺ in the precursor compound. It has to be emphasized that small intensities of the gold oxide and of elemental gold are already present in the low-temperature spectra. Obviously some decomposition of the compound is not avoidable during the preparation of the sample for the measurement. Nevertheless, the three different measurements (DSC/DTA/TG, TDS, and XPS) are highly congruent and present a clear view of the thermal behavior of (NO)[Au(NO₃)₄]. It shows that even for gold, the decomposition proceeds via an oxide as intermediate. However, in contrast to the palladium and platinum compound, this oxide decomposes immediately to elemental gold. Presently we are investigating whether (NO)[Au(NO₃)₄] can also be used in electron-beam-induced decomposition reactions in analogy to its NO₂⁺ congener, and also whether mixtures of the gold compound and its palladium or platinum analogues are suitable for decomposition to give defined alloy structures.

Experimental Section

N₂O₅: Pure N₂O₅ was prepared by dehydration of fuming HNO₃ with P₄O₁₀ according to Ref. [21]. During the dehydration, a constant stream of ozone (ca. 5% in flowing O₂) was passed through the apparatus, and the resulting N₂O₅ was directly condensed into the reaction flasks.

(NO)₂[Pd(NO₃)₄]: Palladium powder (0.053 g) was filled into a 250 mL glass flask. The flask was cooled to -70 °C and N₂O₅ in excess was condensed onto the metal powder. The flask was sealed and allowed to warm up to room temperature. During that time, the metal reacted under formation of a red-brown solution and a brown gas (NO₂). From the solution, well-developed orange-red single crystals separate over the course of five days. By purging with dry N₂, remaining N₂O₅ as well as other volatile reaction products were removed and the product was transferred to a glove box.

(NO)[Au(NO₃)₄]: The same procedure as described for (NO)₂[Pd(NO₃)₄] was repeated using gold powder (0.050 g). The metal dissolved rapidly, and within three days yellow plate-like single crystals grew, which were also handled in a glove box after unreacted N₂O₅ and other volatile products had been removed with N₂.

(NO)₂[Pt(NO₃)₄]: H₂[Pt(OH)₆] was prepared according to Ref. [19], and the compound (109 mg) was reacted with N₂O₅ as described above. Yellow single crystals started to grow shortly after the reaction has finished. It turned out that the crystals decompose readily when the remaining N₂O₅ was removed completely. Therefore some N₂O₅ was kept in the flask for storage purposes.

X-ray crystallography: In a glove box, suitable single crystals of all of the compounds were transferred into perfluorinated protecting oil. Finally they were mounted onto glass fibers and directly placed into the cold N₂ stream (-120 °C) of the diffractometer cooling

device. After unit cell determination, the reflection intensities were collected.^[22] For (NO)₂[Pd(NO₃)₄] and (NO)[Au(NO₃)₄], powder diffraction measurements were performed. For that purpose, finely grounded samples were filled in glass capillaries, which were sealed and measured with Cu_{Kα} radiation using the STADI P powder diffractometer. The data were handled with the software package for the STOE powder diffraction system (WIN X^{POW} 3.01, Stoe & Cie, Darmstadt, Germany, 1996). Owing to the above-mentioned decomposition, no powder pattern of (NO)₂[Pt(NO₃)₄] could be obtained.

DTA/TG measurements: The thermal decomposition of the nitrates was investigated using a TGA/SDTA851^e apparatus (Mettler-Toledo GmbH, Schwerzenbach, Switzerland). (NO)₂[Pd(NO₃)₄] or (NO)[Au(NO₃)₄] (ca. 10 mg) was filled in corundum crucibles in a glove box. For the platinum compound, measurements were performed on samples containing some amounts of N₂O₅ to avoid decomposition prior to the measurement. All of the samples were heated with a rate of 4 K min⁻¹ up to 900 °C. The collected data were processed using the software of the analyzer (STARe V8.1, Mettler-Toledo, Schwerzenbach, 2004).

DSC measurements: For (NO)[Au(NO₃)₄], DSC measurements were performed in a DSC-204 PhoenixTM cell (Netzsch GmbH, Selb, Germany) using a TASC 414/3A controller. For the measurement, the sample (4 mg) was prepared in corundum crucibles equipped with perforated lids. The heating rate was 5 K min⁻¹ and the data were handled using the program of the device (Netzsch Instrumental Software Version 3.5).

TDS measurements: The precursor decomposition was carried out by heating the silicon wafer, which was coated with a solution of (NO)[Au(NO₃)₄] in N₂O₅, with steps of 15 K up to 350 °C. Debuting gases were characterized by a quadrupole mass spectrometer (Pfeiffer QMS/QMA-200). The data were handled with the spectrometer software (Quadstar 422).

X-ray photoelectron spectroscopy (XPS): The spectra of a precursor-coated silicon wafer were obtained at steps of ca. 10 K (in accordance with the observed TDS data) in an ultrahigh vacuum chamber (base pressure of 3 × 10⁻¹⁰ hPa). The sample was irradiated by Mg K_{α1,2} photons (kinetic energy 1253.6 eV) generated by a SPECS XR-50 X-ray gun. The emitted electrons were analyzed by a hemispheric energy analyzer (Leybold EA-10) and detected with an electron multiplier system (Leybold).

Received: August 29, 2011

Published online: January 27, 2012

Keywords: analytical methods · nitrates · noble metals · photoelectron spectroscopy

- [1] T. Ishida, M. Haruta, *Angew. Chem.* **2007**, *119*, 7288; *Angew. Chem. Int. Ed.* **2007**, *46*, 7154.
- [2] A. S. K. Hashmi, G. J. Hutchings, *Angew. Chem.* **2006**, *118*, 8064; *Angew. Chem. Int. Ed.* **2006**, *45*, 7896.
- [3] G. C. Bond, D. Thompson, *Catal. Rev. Sci. Eng.* **1999**, *41*, 319.
- [4] M. Haruta, *Catal. Surv. Jpn.* **1997**, *1*, 61.
- [5] M. J. Kahlich, H. A. Gasteiger, R. J. Behm, *J. Catal.* **1999**, *182*, 430.
- [6] S. Graells, R. Alcubilla, G. Badenes, R. Quidant, *Appl. Phys. Lett.* **2007**, *91*, 121112.
- [7] J. Messelhäuser, E. B. Flint, H. Suhr, *Appl. Phys. A* **1992**, *55*, 196.
- [8] J. Haight, M. R. Aylett in *Laser Microfabrication-Thin Film Processes and Lithography* (Eds.: D. J. Ehrlich, J. Y. Tsao), Academic Press, San Diego **1989**, p. 453.
- [9] A. N. Broers, W. W. Molzen, J. J. Cuomo, N. D. Wittels, *Appl. Phys. Lett.* **1976**, *29*, 596.
- [10] P. Hoffmann, I. Utke, F. Cicoria, *10th Int. Symp. "Nanostructures: Physics and Technology"*, St. Petersburg, Russia, **2002**.

- [11] N. Silvis-Cividijan, *Electron Beam Induced Nanometer Scale Deposition*, Delft University Press, Delft, Niederlande, **2002**.
- [12] A. Folch, J. Tejada, C. H. Peters, M. S. Wrighton, *Appl. Phys. Lett.* **1995**, *66*, 2080.
- [13] T. H. Baum, C. R. Jones, *Appl. Phys. Lett.* **1985**, *47*, 538.
- [14] T. H. Baum, C. R. Jones, *J. Vac. Sci. Technol. B* **1986**, *4*, 1187.
- [15] T. H. Baum, E. E. Marinero, C. R. Jones, *Appl. Phys. Lett.* **1986**, *49*, 1213.
- [16] M. S. Wickleder, O. Büchner, F. Gerlach, M. Necke, K. Al-Shamery, T. Wich, T. Luttermann, *Chem. Mater.* **2008**, *20*, 5181.
- [17] C. C. Addison, G. S. Brownlee, N. Logan, *J. Chem. Soc. Dalton* **1972**, 1440; C. C. Addison, *Chem. Rev.* **1980**, *80*, 21.
- [18] T. Wich, K. Al-Shamery, T. Luttermann, M. Wickleder, F. Gerlach, M. Necke, H. Schnars, O. Büchner, German Patent 102007018845.7–45, **2007**.
- [19] G. Brauer, *Handbuch der Präparativen Anorganischen Chemie*, Ferdinand Enke Verlag, Stuttgart, **1975**, p. 1719.
- [20] Z. Mazej, M. Ponikvar-Svet, J. F. Liebman, J. Passmore, H. D. Brooke Jenkins, *J. Fluorine Chem.* **2009**, *130*, 788.
- [21] G. Brauer, *Handbuch der Präparativen Anorganischen Chemie*, Ferdinand Enke Verlag, Stuttgart, **1975**, p. 473.
- [22] Measurements: STOE IPDS I (for Au and Pd), BRUKER κ -APEX2 (for Pt), $\lambda(\text{MoK}\alpha) = 71.073$ pm, $T = 153$ K; Computing: structure solutions by direct methods, full-matrix least-square refinements, programs SHELXS-97 and SHELXL-97 (G. M. Sheldrick, Göttingen **1997**), numerical absorption corrections with X-RED 1.22 and X-SHAPE 1.06 (Stoe, Darmstadt **2001** and **1999**); Crystal data: (NO)[Au(NO₃)₄]: Yellow block (0.55 × 0.38 × 0.37 mm³), monoclinic, $P2_1/n$, $Z = 2$, $a = 827.01(9)$, $b = 726.38(9)$, $c = 909.20(10)$ pm, $\beta = 111.907(10)^\circ$, $506.74(10)$ Å³, $\rho = 3.133$ g cm⁻³, $2\theta_{\text{max}} = 52.34^\circ$, 6208 reflections, 1000 unique reflections ($R_{\text{int}} = 0.1064$), $\mu = 146.11$ cm⁻¹, min./max. transmission = 0.0459/0.0745, 89 parameters, $R_1 = 0.0342$, $wR_2 = 0.0618$ for all reflections, max./min. residual electron density = 1.620/−1.495 e⁻ Å⁻³. (NO)₂[Pd(NO₃)₄]: Red plate (0.40 × 0.15 × 0.07 mm³), monoclinic, $P2_1/c$, $Z = 2$, $a = 806.93(9)$, $b = 747.31(5)$, $c = 917.08(10)$ pm, $\beta = 99.372(13)^\circ$, $545.64(9)$ Å³, $\rho = 2.523$ g cm⁻³, $2\theta_{\text{max}} = 56.50^\circ$, 7773 reflections, 1266 unique reflections ($R_{\text{int}} = 0.0514$), $\mu = 18.80$ cm⁻¹, min./max. transmission = 0.5316/0.8839, 97 parameters, $R_1 = 0.0215$, $wR_2 = 0.0446$ for all reflections, max./min. residual electron density = 0.468/−0.678 e⁻ Å⁻³. (NO)₂[Pt(NO₃)₆]: Yellow block (0.41 × 0.23 × 0.21 mm³), monoclinic, $P2_1/c$, $Z = 2$, $a = 711.38(2)$, $b = 934.96(3)$, $c = 1156.68(4)$ pm, $\beta = 107.559(2)^\circ$, $733.48(4)$ Å³, $\rho = 2.840$ g cm⁻³, $2\theta_{\text{max}} = 56.60^\circ$, 12740 reflections, 3041 unique reflections ($R_{\text{int}} = 0.0596$), $\mu = 97.09$ cm⁻¹, min./max. transmission = 0.1097/0.2350, 134 parameters, $R_1 = 0.0258$, $wR_2 = 0.0734$ for all reflections, max./min. residual electron density = 4.068/−2.172 e⁻ Å⁻³. Further details on the crystal structure investigation may be obtained from the Fachinformationszentrum Karlsruhe, 76344 Eggenstein-Leopoldshafen, Germany (fax: (+49)7247-808-666; e-mail: crysdata@fiz-karlsruhe.de), on quoting the depository numbers CSD-423407 (NO)[Au(NO₃)₄], 423406 (NO)₂[Pd(NO₃)₄], and 423405 (NO)₂[Pt(NO₃)₆].
- [23] B. V. Crist in *PDF Handbook of Monochromatic XPS-Spectra*, Vol. 2, XPS International, **2005**, p. 75–83.
- [24] Q. Fu, H. Saltsburg, M. Flytzani-Stephanopoulos, *Science* **2003**, *301*, 935.